AUTO LOAD-LEVELLING CONTROL OF A LARGE SPRAYER CHASSIS USING THE SLIDING MODE METHOD

/

基于滑模控制的大型喷雾机底盘自动调平方法研究

Yu Chen[1)], Jun Wu[2)], Shuo Zhang[1)], Jun Chen*[1)], Hui Xia[3)], Yahui Zhu [3)], Jiajun Wang [3)]

[1)] College of Mechanical and Electronic Engineering, Northwest A&F University, Yangling 712100, China;

[2)] Nanjing Research Institute for Agricultural Mechanization, Ministry of Agriculture and Rural Affairs, Nanjing 210014, China;

[3)] Jiangsu World Agriculture Machinery Co., Ltd, Danyang 212300, China;

Tel: +86 13572191773; E-mail: chenjun_jdxy@nwsuaf.edu.cn

DOI: https://doi.org/10.356.33/inmateh-64-06

Keywords: *Agricultural sprayer, Sliding mode variable structure, Air suspension, Auto load levelling control*

ABSTRACT

When a sprayer travels on a ramp or a rough road, the load exerted on each wheel changes. If an unbalanced wheel load is maintained for long periods of time, the wheels may slip, the sprayer's manoeuvrability is affected, and a rollover accident may occur. In this study, the air suspension of a self-propelled sprayer chassis was investigated, and the potential load imbalance conditions of the sprayer suspension were analysed. A mathematical model of the inflation/deflation of the suspension was established based on air nonlinear thermodynamics and vertical dynamics theory and a ¼-scale vertical dynamics model of the sprayer chassis was developed. A control strategy to balance the sprayer's wheel load was developed. Considering the nonlinear characteristics of the air suspension, a sliding mode variable structure control method was used to balance the wheel load. Simulation experiments were conducted under different working conditions. The simulation results showed that the sliding mode variable structure control provided good control response and precision. The proposed auto load-levelling controller was tested under different working conditions, including different roll and pitch angles and navigating a rough road; the controller successfully changed the load on each spring to ensure that the sprung mass of the suspension was equal and the wheel load was balanced. The results of this study provide reference information for auto load-levelling control of large sprayers.

摘要

喷雾机在凹凸路面或者坡道路面行驶时，导致各车轮负载会发生变化。长时间车轮负载的不平衡，不仅会使车轮出现打滑或失去操纵能力，更会导致侧翻事故的发生。本文以带空气悬架的大型高地隙自走式喷雾机为研究对象，分析喷雾机车轮可能发生载荷不平衡的工况。基于车辆动力学和空气热力学理论，建立了空气悬架充放气数学模型和 1/4 悬架垂向动力学模型。在此基础上，制定了喷雾机车轮负载平衡控制策略。考虑到空气悬架的非线性特性，采用滑模变结构控制，设计了车轮负载平衡控制器，并以不同工况为例，进行了仿真对比实验。通过仿真实验可以得到，滑模控制对模型参数的变化具有较好的鲁棒性，使其具有良好的控制响应和精度。同时，在侧倾、俯仰和凹凸路面三种工况下，通过本文设计的负载平衡控制器的干预和控制，各弹簧所受载荷也随之变化，最终使得整机左右两侧悬架簧载质量相等，各车轮负载达到平衡状态。通过本文研究，可为大型高地隙自走式喷雾机车轮负载平衡控制提供参考。

INTRODUCTION

As an important tool for preventing and eliminating crop diseases and insect pests, pesticide applications have become an important measure to improve crop yield (*Li X. et al., 2017*). The self-propelled sprayer is an essential piece of equipment to ensure secure food production and stable development of agriculture (*Tahmasebi M. et al., 2013; 2018*). With the advancement of agricultural mechanization and the implementation of large-scale farm cooperative management, high-power and high-efficiency field management machinery is needed to spray and fertilize large plots. An advanced sprayer with excellent performance allows for the precise, efficient, and intelligent management of field crops and has the characteristics of high efficiency, low injury risk, field friendliness, good comfort, and mobility. High-clearance self-propelled sprayers are important for spraying and fertilizing crops and are widely used due to their high efficiency, environmental protection capacity, and ease of use (*Chen Y. et al., 2020; Yuki S. et al., 2013; Baumhardt U. B. et al., 2017*).

Compared with the general agricultural machinery, the sprayer has complicated operating conditions and needs to be equipped with a special suspension system to improve its ride comfort, reduce the vibration, swing and rotation of the sprayer boom, thereby making the spray more uniform and reduce drift (*Herbst A. et al., 2018; Ilica A. et al., 2018; Gil E. et al., 2015*). Air suspension is widely used in sprayers because of its good nonlinear elastic characteristics, large suspension range, adjustable load capacity, and large load-bearing mass (*Melzi S. et al., 2014; Chen Y. et al., 2016*). Some sprayer manufacturers such as John Deere (*Carlson B. C. et al., 2011; Wubben T. M. et al., 2007*) and Hagie (*Schaffer J. A., 2002*) use a four-wheel independent vertical shaft air suspension system. A vertical shaft is connected between the wheel hub and the bottom of the airbag and the top of the airbag is attached to a sleeve connected to the vehicle frame through a gantry frame. As the sprayer travels over uneven road surfaces, the air springs are squeezed and stretched to reduce suspension buffer vibration. In order to ensure that the sprayer is adaptable to complex operating conditions, researchers have focused on the active or semi-active adjustment of the suspension by attaching an adjustable damper to the suspension, adding a highly stable device to the elastic element, or integrating a ground clearance adjustment device into the suspension (*Zatrieb J. et al., 2012; Li W. et al., 2018*).

A large self-propelled sprayer has a high operating speed and high ground clearance; the sprung mass and the content of the liquid change frequently during the spraying process (*Chen Y. et al., 2012*). The sprayer mass is in the range of ten to twenty tons and the width of the spray rod is twenty to fifty meters, significantly exceeding the size of regular vehicles and off-road vehicles (*Cui L. F. et al., 2018; 2019*). The sprayer is not only different from road vehicles, but also different from general non-road vehicles. When the sprayer is in the transport condition, the fast running speed requires that the sprayer suspension can fully dissipate the vibration energy transferred from the ground to the body to ensure sprayer comfort and smoothness. When the sprayer is in the spraying condition, the ground friendliness should be taken into account, that is, the excessive dynamic tire load should not be generated to prevent soil compaction and damage. When the sprayer is in the injection or spraying conditions, the body mass will change, at this time the suspension can adjust the body height in real time to ensure the driving stability. In addition, since the sprayer mostly adopts the "two pump + four motor" full hydraulic driving scheme, each wheel should have enough load to prevent wheel slip and tire wear. However, when the sprayer is driving on a ramp, the machine mass will shift to one side, which increases the wheel load on the lower side and the risk of overloading the wheel. The load is lower on the high side and the wheels may slip or lose control. Due to the high barycentre of high-clearance sprayers and the unbalanced load on both sides of the wheels, rollover accidents can easily occur. The imbalance of the wheel load not only has a large influence on the handling stability and safe operation of the sprayer but also affects the quality and efficiency of the sprayer operation. Therefore, measures must be taken to eliminate or reduce this effect.

In order to ensure the vehicle running stability and safety, researchers have studied the vehicle body height stability control and made some progress. Holbrook developed a method for the manual and automatic adjustment of the sprung mass height of the suspension to a predetermined reference height (*Holbrook G., 2010*). Hyunsup (*Kim H. et al., 2011*) applied the sliding mode control theory to design a non-linear controller for an air suspension based on body height adjustment. The controller monitored the height change of the car body in real time using a pressure sensor installed inside the four air springs and adjusted the height (height control) and the roll angle and pitch angle of the car body (levelling control). Simulations and experiments indicated that the controller improved the ride comfort and safety. In addition, electronically controlled air suspension systems have the disadvantages of overcharge, over-discharge, and sensor failure. Jang (*Jang I. et al., 2007*) used a failure protection algorithm to perform auxiliary correction control on the target height of the vehicle body. Yang conducted a detailed study on the relationship between the stiffness and height of the air spring and air charging and discharging and designed an electronically controlled air suspension system based on fuzzy proportional-integral-derivative (PID) control (*Yang Q. Y., 2008*). Wang conducted an analysis of the characteristics of the charge and discharge process of an air spring and divided the vehicle body height into high, medium, and low. A fuzzy control algorithm was used to control the vehicle body height depending on the road surface and speed of the vehicle (*Wang S. H. et al., 2013*).

However, these researches mainly focused on the control of the vehicle body height (*Wang S. H. et al., 2015; Jiang H. et al., 2015*), and there are few studies on the auto load-levelling control of agricultural sprayers. When the height of air suspension, hydropneumatic suspension and other nonlinear suspension is controlled, due to the strong nonlinearity and the variability of the suspension internal parameters, the general control method effect has a certain overshoot phenomenon (*Jiang H. et al., 2017; Chen Y. X. et al.,*

2015; Porumamilla H. et al., 2005). The large high clearance self-propelled sprayer chassis mostly use air suspensions, the driving road conditions and operating conditions are complex and changeable. The precision and response speed of auto load-levelling control directly affect the safety and spray quality of the sprayer.

Therefore, in this study, the air suspension of a self-propelled sprayer chassis was taken as the object and potential load imbalance conditions of the sprayer suspension were analysed. An auto load-levelling control strategy of the sprayer chassis air suspension was developed. According to the nonlinear characteristics of air inflation/deflation process and law of gas thermodynamics, the mathematical model of the air spring inflation/deflation and ¼-scale vertical dynamic model of sprayer chassis air suspension were established. Based on the differential geometry theory, the ¼-scale suspension vertical dynamic model was globally linearized by the state feedback linearization method, and the sliding mode controller was designed in the linear domain. Through the inverse linear transformation, a nonlinear control algorithm for sprayer auto load-levelling in the original coordinate system was obtained. The simulation results show that the developed auto load-levelling control strategy and algorithm can efficiently and accurately control the load levelling of the high-clearance sprayer chassis suspension under various unfavourable working conditions to ensure the stability and safety of the sprayer.

MATERIALS AND METHODS

Analysis of sprayer operating conditions

In certain road conditions, the vertical load of the wheels will change, thereby reducing the adhesion of the wheels to the ground or a wheel(s) may not touch the ground. As shown in Fig. 1(a), it is assumed that when the sprayer is running, the rear left wheel enters a pit and the wheel is not suspended due to the use of an independent air suspension. Under the action of air pressure inside the air spring, the air spring is rapidly stretched. Therefore, the internal pressure and the load borne by the spring also decrease, ultimately reducing the adhesion of the wheel. This impacts the handling performance of the sprayer. Due to the use of a hydrostatic drive, when a drive wheel has less adhesion, the driving force is greater than the adhesion and the wheel will slip. Tire skid not only consumes a lot of power but also increases tire wear and soil damage. When the sprayer is driving on a ramp, as shown in Fig. 1(b), the mass of the machine will shift to one side, increasing the wheel load on the lower side and the risk of overloading the wheel. The load on the high side is reduced and the wheels may slip or lose control. Due to high barycentre of the high-clearance sprayer and the unbalanced load on both sides of the wheels, rollover accidents can easily occur. The load imbalance is caused by a change in the attitude of the sprayer body. When the sprayer body is in the levelling state, the mass of the body is distributed to each suspension system with equal mass. Since the suspensions are directly connected to the wheels, the load on each wheel is also equal. Therefore, the load balancing process of the sprayer wheel is equivalent to the process of its body levelling.

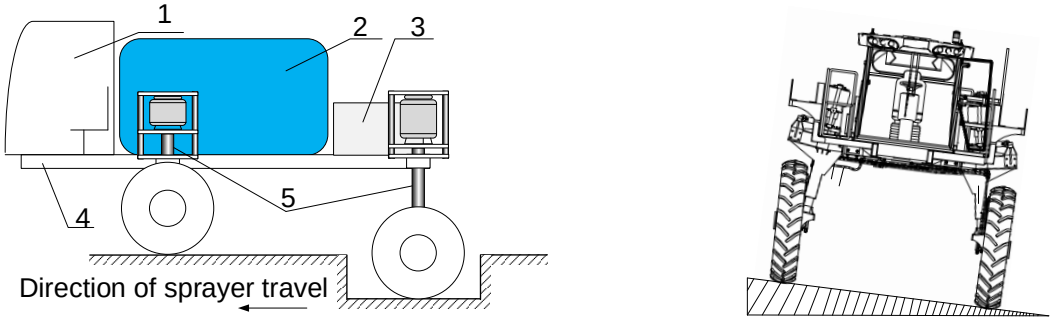

(a) Sprayer is driving on uneven roads *(b) Sprayer is driving on a ramp*

1. cab; 2. liquid tank; 3. engine; 4. frame; 5. pneumatic suspension

Fig. 1 – Schematic diagram of load imbalance

Mathematical model

The air suspension of the sprayer chassis is inflated and deflated to adjust the body attitude and achieve load-levelling. In order to adjust the sprayer's load balance, a pneumatic system was designed, as shown in Fig. 2.

The pneumatic system consists of an air compressor, a pressure-regulating valve, an air dryer, an accumulator, four height sensors, four three-position three-way proportional solenoid valves, four air springs, and an air spring control unit. The compressed air required by the system is provided by an air compressor

on the engine. The air compressor supplies clean, dry compressed air to the suspension system in an appropriate pressure range while ensuring that the air compressor has a suitable load condition and the impact on the engine performance is low. The pressure regulator switches between the operating and unloading state of the air compressor to regulate the system pressure. The air dryer absorbs moisture from the air and prevents the system components from getting wet. It can also be used to filter oil mist and particulate impurities in the air and to alleviate system component wear. The function of the accumulator is to buffer and store energy so that the air enters the suspension system smoothly.

The height sensor is installed beside each air spring. The controller controls the movement of the solenoid valve spool through an electrical signal output by the sensor to charge and discharge the air spring, adjust the height of the air spring, and achieve load-levelling of each wheel. When the height of the sprayer is increased by the air spring, the air passes from the accumulator and three-position three-way solenoid valve to the air spring. When the height is reduced, the air flows out from the air spring, passes through the three-position three-way solenoid valve, and then is vented to the atmosphere by an exhaust valve. Therefore, the mathematical model of the system includes three parts: the accumulator model, the fluid resistance model, and the air spring model.

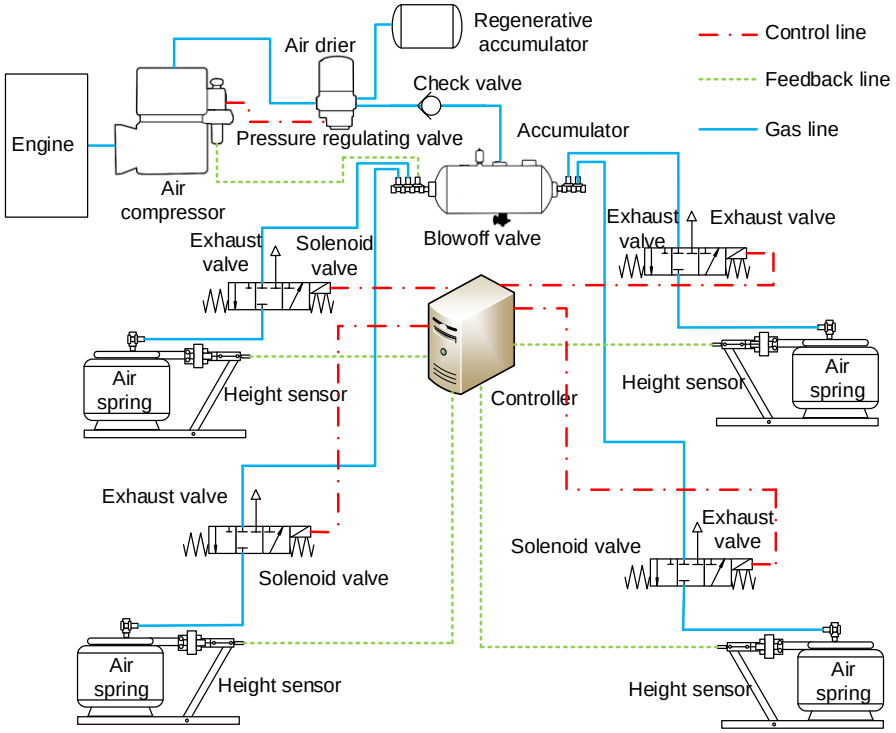

Fig. 2 - Schematic diagram of sprayer airflow line system

- **Accumulator model**

As the constant volume air source of the suspension system, the accumulator's charging process of the air spring can be regarded as a constant-volume air discharge process. The airflow out of the accumulator is considered negative airflow. Based on the mass continuity equation and the ideal gas state equation, it can be concluded that during the inflation of the air spring, the gas pressure changes in the accumulator are defined as:

$$\dot{p}_c = -\frac{nRT_{c0}}{V}\left(\frac{p_c}{p_{c0}}\right)^{\frac{n-1}{n}} G_c \tag{1}$$

In Eq. (1), p_c, T_{c0}, and p_{c0} are the absolute pressure, initial gas temperature and absolute pressure in the accumulator, respectively; the units are MPa, K, and MPa; V is the accumulator volume, m^3; refer to literature (*Carneiro J. F. et al., 2006*), the thermodynamic charging / discharging of air inside pneumatic suspensions are regarded as a polytropic process, n is the gas polytropic index that can be adjusted from 1 (isothermal process) to 1.4 (adiabatic process). According to literature (*Carneiro J. F. et al., 2006*), the value of n is 1.35 as a calculation example; R is a constant and the value is 287.1 J/(kg·K).

- **Fluid resistance model**

The air flows through the solenoid valves and the gas lines produce fluid resistance. The pressure-flow characteristics when airflow passes through the solenoid valve and pneumatic pipeline are equivalent to the pressure-flow characteristics when airflow passes through the throttle valve orifice. Therefore, the mass flow rate of air passing through the solenoid valve and pneumatic pipeline when the suspension is raised is:

$$G_c = \frac{c_d K p_c A_{K1} N_c}{\sqrt{T_c}} \tag{2}$$

When the suspension is lowered, the air in the air spring is directly discharged into the atmosphere through the solenoid valve. Therefore, the mass flow rate when air passes through the solenoid valve and the pneumatic pipe is:

$$G_k = -\frac{c_d K p_1 A_{K1} N_k}{\sqrt{T_1}} \tag{3}$$

where K is taken as a constant, which is a function of the polytropic exponent n for air. N_c and N_k are restriction factor, which are function of n and the up-stream and down-stream pressures.

When the suspension is raised, the up-stream and down-stream pressures are P_c and P_1, respectively.

When the suspension is lowered, the up-stream and down-stream pressures are $P1$ and P_a, respectively. T_c and T_1 are gas temperature in the Accumulator and air spring, respectively, the units are K. N_c, N_k, K can be obtained by the following formulas.

$$N_c = \left\{ \frac{\left(\frac{p_1}{p_c}\right)^{\frac{2}{n}} - \left(\frac{p_1}{p_c}\right)^{\frac{n+1}{n}}}{\frac{(n-1)}{2}\left(\frac{2}{n+1}\right)^{\frac{n+1}{n-1}}} \right\}^{\frac{1}{2}}, \quad N_k = \left\{ \frac{\left(\frac{p_a}{p_1}\right)^{\frac{2}{n}} - \left(\frac{p_a}{p_1}\right)^{\frac{n+1}{n}}}{\frac{(n-1)}{2}\left(\frac{2}{n+1}\right)^{\frac{n+1}{n-1}}} \right\}^{\frac{1}{2}}, \quad K = \left[\frac{n}{R}\left(\frac{2}{n+1}\right)^{\left(\frac{n+1}{n-1}\right)} \right]^{\frac{1}{2}}$$

- **Air spring model**

When the suspension is raised, a variable-mass variable-volume aeration process occurs in the air spring. The air mass flow from the accumulator to the air spring through the solenoid valve is defined as G_c and the air pressure inside the spring is:

$$\dot{p}_1 = -\frac{n p_1}{V_1}\dot{V}_1 + \frac{n R T_{10}}{V_1}\left(\frac{p_1}{p_{10}}\right)^{\frac{n-1}{n}} G_c \tag{4}$$

Similarly, when the suspension is lowered, a variable-mass variable-volume deflation process occurs in the air spring. The change rate of the gas pressure inside the spring is:

$$\dot{p}_1 = -\frac{n p_1}{V_1}\dot{V}_1 - \frac{n R T_{10}}{V_1}\left(\frac{p_1}{p_{10}}\right)^{\frac{n-1}{n}} G_k \tag{5}$$

- **Vertical dynamic model of sprayer suspension**

Equations (1) to (5) indicate that the vertical dynamics model of the ¼-scale suspension during inflation and deflation is:

When the spring is inflated

$$\begin{cases} G_c = \dfrac{c_d K p_c A_{K1} N_c}{\sqrt{T_c}} \\ \dot{p}_c = -\dfrac{n R T_{c0}}{V}\left(\dfrac{p_c}{p_{c0}}\right)^{\frac{n-1}{n}} G_c \\ \dot{p}_1 = -\dfrac{n p_1}{V_1}\dot{V}_1 + \dfrac{n R T_{10}}{V_1}\left(\dfrac{p_1}{p_{10}}\right)^{\frac{n-1}{n}} G_c \\ m_b(\ddot{x}_b + g) + c_s(\dot{x}_b - \dot{x}_t) = (p_1 - p_a)A_e \\ m_t\ddot{x}_t - c_s(\dot{x}_b - \dot{x}_t) - m_b g + k_t(x_t - w) + c_t(\dot{x}_t - \dot{w}) = -(p_1 - p_a)A_e \end{cases} \tag{6}$$

$$\text{When the spring is deflated}\begin{cases} G_k = -\dfrac{c_d K p_1 A_{k1} N_k}{\sqrt{T_1}} \\ \dot{p}_1 = -\dfrac{n p_1}{V_1}\dot{V}_1 - \dfrac{nRT_{10}}{V_1}\left(\dfrac{p_1}{p_{10}}\right)^{\frac{n-1}{n}} G_k \\ m_b(\ddot{x}_b + g) + c_s(\dot{x}_b - \dot{x}_t) = (p_1 - p_a)A_e \\ m_t\ddot{x}_t - c_s(\dot{x}_b - \dot{x}_t) - m_b g + k_t(x_t - w) + c_t(\dot{x}_t - \dot{w}) = -(p_1 - p_a)A_e \end{cases} \quad (7)$$

In Eqs. (1) to (7), p_a is atmospheric pressure and the value is 0.1 MPa; the other unmarked symbols meanings are listed in Tab.1.

Table 1

Symbols meaning in Eqs. (1) to (7)

Symbols/unit	Instructions	Symbols/unit	Instructions
p_c/ MPa	Absolute pressure in the accumulator	T_{c0}/ K	Initial gas temperature in the accumulator
p_{c0}/ MPa	Initial absolute pressure in the accumulator	V/ m^3	accumulator volume
c_d	Throttle valve shrinkage coefficient	A_{k1}/ m^2	The solenoid valve port area
T_c / K	Gas temperature in the accumulator	T_1/ K	Gas temperature in the air spring
p_1 / MPa	Absolute pressure in the air spring	m_b/ kg	Sprung mass
g / m·s^{-2}	Gravity acceleration	m_t/ kg	Unsprung mass
x_b/ m	Sprung mass displacement	x_t/ m	Unsprung mass displacement
V_1/ m^3	Air spring volume	C_s/ N·s·m^{-1}	Suspension damping
T_{10}/ K	Initial gas temperature in the air spring	p_{10}/ MPa	Initial pressure in the air spring
k_t/ N·m^{-1}	Tire equivalent radial stiffness	A_e/ m^2	Effective cross-sectional area of the air spring
w/ m	Road excitation	C_t/ N·s·m^{-1}	Tire equivalent radial damping

Controller design

- **Control strategy**

During automatic load-levelling, the adjustment range needs to be set in advance, as shown in Fig. 3. D_t is the adjustment amount. The value of D_t is related to the height difference between springs. D_t is obtained using Eq. (8).

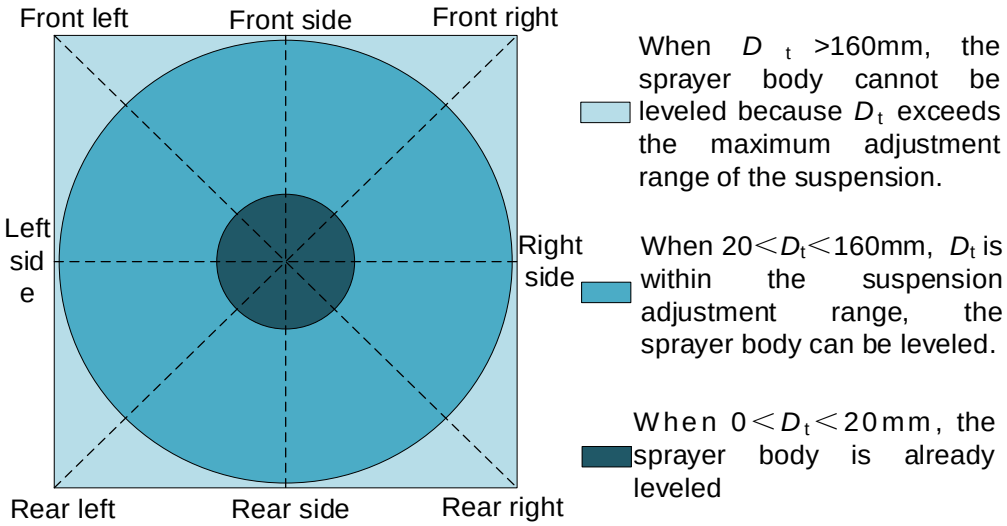

Fig.3 - Schematic diagram of load levelling adjusting range

$$D_t = \begin{cases} \max(x_{bij}) - \min(x_{bij}) & \text{When the four springs are individually adjusted} \\ \varphi L & \text{When the sprayer climbs or downhill} \\ \theta B_F & \text{When the sprayer drives along the ramp} \end{cases} \quad (8)$$

In Eq. (8), *ij* represents the four positions of the suspensions relative to the sprayer chassis, which is denoted as *FL, FR, RL*, and *RR. FL, FR, RL*, and *RR* represent front left, front right, rear left, rear right, respectively. θ and φ are the sprayer body roll angle and pitch angle measured by a gyroscope. L and B_F are the wheelbase and wheel track respectively. According to the load balancing requirements, combined with the characteristics of the air suspension structure, a load balancing control strategy for the large high-clearance self-propelled sprayer is developed. The strategy is shown in Fig. 4. The high-frequency and low-frequency limits of the bandpass filter are 0.05 Hz and 0.1 Hz, respectively. The bandpass filter filters out changes in body displacement caused by road surface excitation and sprung mass changes. The BLOCKTIMER allows the controller to compare changes in the adjustment D_t within 10 s to identify whether the sprayer is in a long-term load imbalance condition and makes adjustments to avoid frequent movement of the solenoid valve. In the initial state, the height difference of each spring is within 20 mm and the loads of the springs are in equilibrium. When the sprayer travels on uneven roads or slopes, the loads of the springs change under the weight of the body. When the height difference between springs caused by the load change is within the range of 20 mm, the controller recognizes that the sprayer is in a balanced load state. When the height difference between springs exceeds 160 mm, the controller alerts the driver that the machine load is not in the equilibrium state so that the driver uses caution when operating the sprayer. When the height difference between springs is in the range of 20~160 mm, the sprayer is in a load level state. In addition to the height sensor, a gyroscope is installed at the barycentre of the sprayer. The gyroscope measures the tilt angle of the sprayer in the front and rear directions or the left and right directions when the sprayer is operated on a slope. The controller calculates D_t based on the measured tilt angle and the wheelbase and wheel track of the sprayer. During load-levelling, the spring on the high side has priority of deflation and if load-levelling cannot be achieved, the spring on the low side is inflated. High side refers to the side with large sprung mass displacement value x_{bij} in the four suspensions of sprayer. Low side refers to the side with small sprung mass displacement value x_{bij} in the four suspensions of sprayer. Reducing the inflation time of the spring reduces the pumping time of the air compressor and extends the life of the compressor.

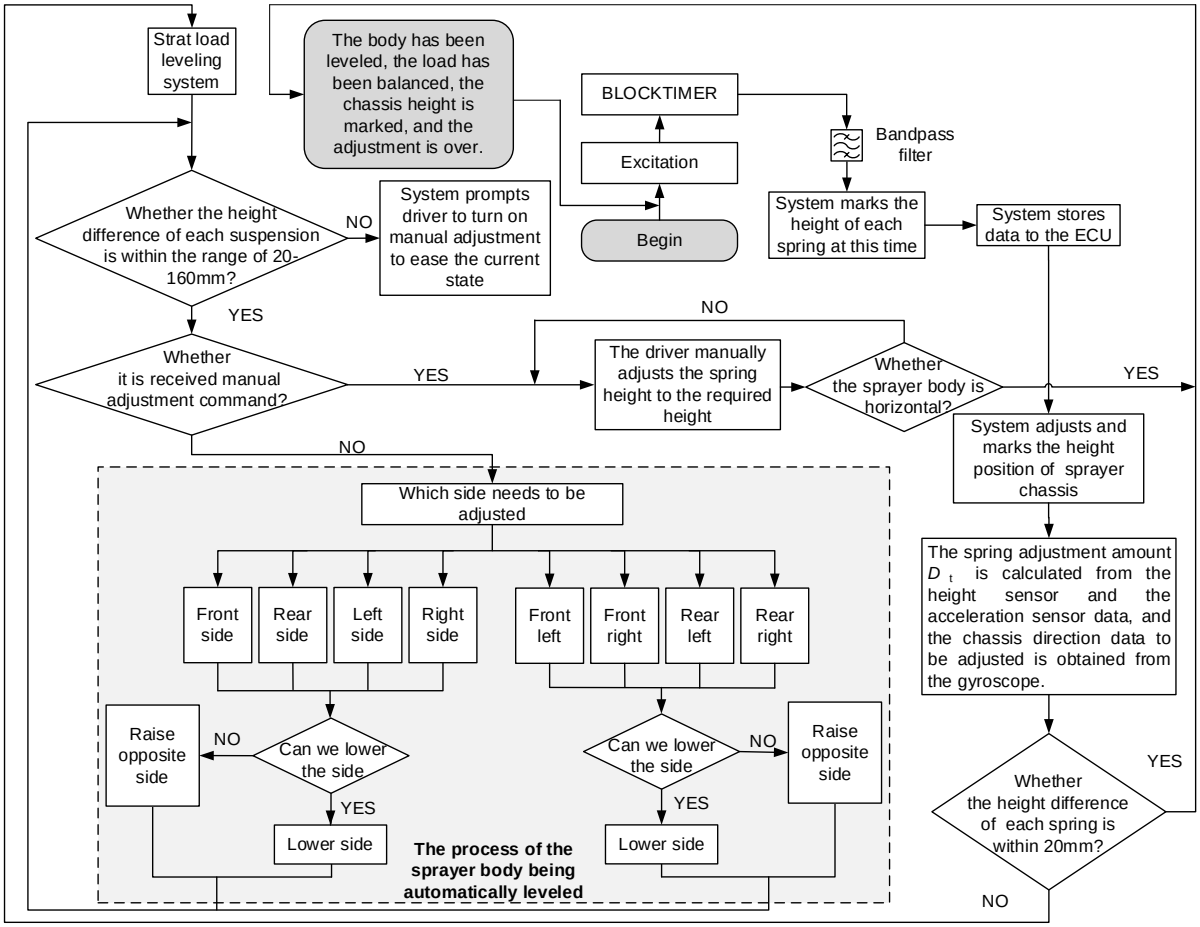

Fig. 4 - Control strategy of auto load levelling

- **Control algorithm**

The auto load-levelling control is based on the suspension height and body attitude, which are determined by the height sensors, the unsprung mass acceleration sensors, and the gyroscope. The amount of adjustment required for each spring is calculated and the springs are adjusted to achieve load-levelling of the suspensions. Therefore, auto load-levelling control requires a control algorithm to adjust the target height. The established load-levelling control strategy and the sliding mode control are used for the proposed auto load-levelling control algorithm, which is shown in Fig. 5. The u_{ij} is the control amount and x_{bijm} is the target height of each spring. In order to obtain the sprung mass displacement x_{bij} of the air suspensions, x_{ij} and x_{tij} need to be obtained. The x_{ij} could be obtained through the spring height sensor, and the x_{tij} could be obtained by the unsprung mass acceleration sensor.

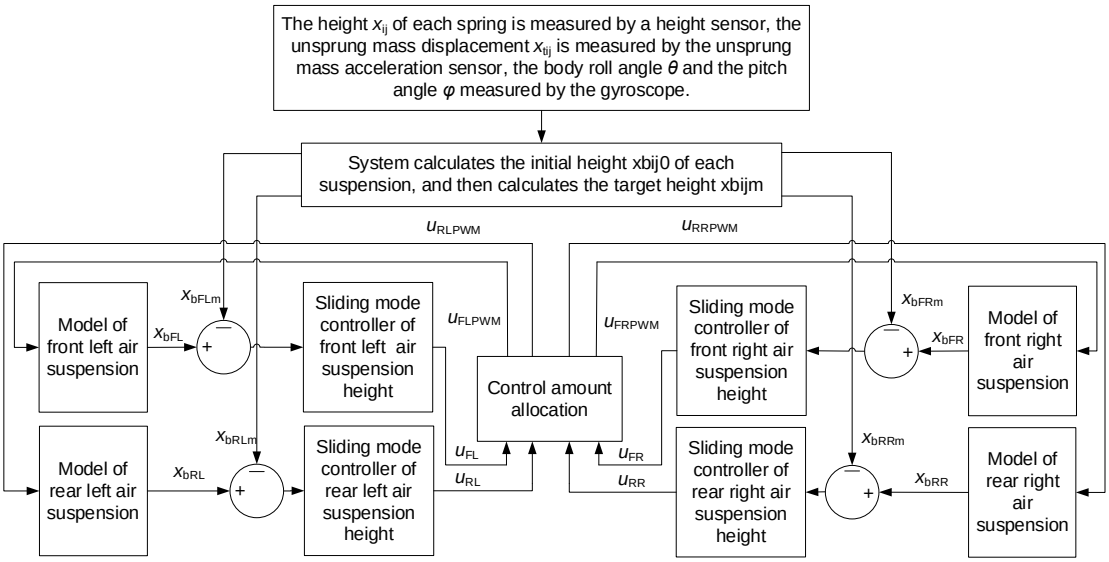

Fig. 5 - Control algorithm of auto load levelling

- **Auto load-levelling control model of the sprayer chassis**

We use the front left air suspension during inflation as an example; the system state variable is $\boldsymbol{x}_{FL}=[x_1\ x_2\ x_3\ x_4\ x_5]^T=[x_{bFL}\ \dot{x}_{bFL}\ x_{tFL}\ \dot{x}_{tFL}\ p_{1FL}]^T$.

The vertical dynamics model of the sprayer suspension model represents the state equation, as shown in Eq. (9).

$$\begin{cases} \dot{\boldsymbol{x}}_{FL} = f(\boldsymbol{x}_{FL}) + g(\boldsymbol{x}_{FL})u_{FL} \\ \boldsymbol{x}_{FL} = \left[x_{bFL} \quad \dot{x}_{bFL} \quad x_{tFL} \quad \dot{x}_{tFL} \quad p_{1FL}\right]^T \\ y = h(\boldsymbol{x}_{FL}) = x_{bFL} - x_{tFL} \end{cases} \tag{9}$$

$f(x_{FL})$ and $g(x_{FL})$ in Eq. (9) are expressed as:

$$f(\boldsymbol{x}_{FL}) = \begin{bmatrix} x_2 \\ \left((x_5 - p_a)A_{eFL} - c_{dFL}(x_2 - x_4) - m_{bFL}g\right)/m_{bFL} \\ x_4 \\ \left(c_{dFL}(x_2 - x_4) - \left((x_5 - p_a)A_{eFL} - m_{bFL}g\right) - k_{tFL}x_3 - c_{tFL}x_4\right)/m_{tFL} \\ -\left(np_{1FL}A_{eFL}(x_2 - x_4)\right)/V_{1FL} \end{bmatrix}, \quad g(\boldsymbol{x}_{FL}) = \begin{bmatrix} 0 \\ 0 \\ 0 \\ 0 \\ nRT_{1FL}/V_{1FL} \end{bmatrix}.$$

According to Eq. (9), Eq. (10) can be obtained from the theory of differential geometry.

$$L_f h(\boldsymbol{x}_{FL})=x_2-x_4,\ L_f^2 h(\boldsymbol{x}_{FL})=f_2-f_4,\ L_g h(\boldsymbol{x}_{FL})=0,$$
$$L_f^3 h(\boldsymbol{x}_{FL})=\left(\left(\frac{1}{m_{bFL}}+\frac{1}{m_{tFL}}\right)\left(A_{eFL}f_5-c_{dFL}f_2+c_{dFL}f_4\right)\right)+\frac{(k_{tFL}+c_{tFL})}{m_{tFL}}(f_3+f_4),\quad (10)$$
$$L_g L_f h(\boldsymbol{x}_{FL})=0,\ L_g L_f^2 h(\boldsymbol{x}_{FL})=\left(\frac{1}{m_{bFL}}+\frac{1}{m_{tFL}}\right)\frac{nRT_{1FL}A_{eFL}}{V_{1FL}}\neq 0$$

According to Eq. (10), the relative order of the system is 3, which is smaller than the order of the equation state of the original system. Therefore, local feedback linearization processing can be performed on Eq. (9). We define the new system state variable $\boldsymbol{\vartheta}_{FL}=[x_{bFL}\text{-}x_{tFL}\ \dot{x}_{bFL}\text{-}\dot{x}_{tFL}\ \ddot{x}_{bFL}\text{-}\ddot{x}_{tFL}]^T$ in linear space. The state equation of Eq. (9) in linear space is as shown in Eq. (11). The relationship between the original control amount u_{FL} and the control amount υ_{FL} in the linear state is defined in Eq. (12).

$$\begin{cases}\dot{\boldsymbol{\vartheta}}_{FL}=\mathbf{A}\boldsymbol{\vartheta}_{FL}+\mathbf{B}\upsilon_{FL}\\ y=\vartheta_{1FL}\end{cases}\quad (11)$$

$$\upsilon_{FL}=L_f^3 h(\boldsymbol{x}_{FL})+L_g L_f^2 h(\boldsymbol{x}_{FL})u_{FL}\quad (12)$$

A and **B** in Eq. (11) are expressed as:

$$\mathbf{A}=\begin{bmatrix}0&1&0\\0&0&1\\0&0&0\end{bmatrix},\ \mathbf{B}=\begin{bmatrix}0\\0\\1\end{bmatrix}.$$

The model obtained by feedback linearization is a third-order linear system. In the linear system, the new output error is defined as $e_{FL}=\vartheta_{1FL}\text{-}\vartheta_{1dFL}$. The sliding surface can be set to:

$$s_{FL}=\lambda_{FL}^2 e_{FL}+2\lambda_{FL}\dot{e}_{FL}+\ddot{e}_{FL}\quad (13)$$

In Eq. (13), λ_{FL} is the sliding mode coefficient and $\lambda_{FL}>0$. The sliding mode control output υ_{FL} consists of an equivalent control amount υ_{FLeq} and a switching control amount υ_{FLsw}, that is,

$$\upsilon_{FL}=\upsilon_{FLeq}+\upsilon_{FLsw}\quad (14)$$

The effect of the equivalent control is to drive the system state to move along the expected sliding mode surface (*Zhao Y. Z. et al., 2014; Jin M. et al., 2014; Assadsangabi B. et al., 2009; Zirkohi M. M. et al., 2015*) and keep the system at $\dot{s}_{FL}=0$. We use the derivative of Eq. (13) to obtain Eq. (15).

$$\begin{aligned}\dot{s}_{FL}&=\lambda_{FL}^2\dot{e}_{FL}+2\lambda_{FL}\ddot{e}_{FL}+\dddot{e}_{FL}\\&=\lambda_{FL}^2\left(\dot{\vartheta}_{1FL}-\dot{\vartheta}_{1dFL}\right)+2\lambda_{FL}\left(\ddot{\vartheta}_{1FL}-\ddot{\vartheta}_{1dFL}\right)+\left(\dddot{\vartheta}_{1FL}-\dddot{\vartheta}_{1dFL}\right)\\&=\lambda_{FL}^2\left(\vartheta_{2FL}-\dot{\vartheta}_{1dFL}\right)+2\lambda_{FL}\left(\vartheta_{3FL}-\ddot{\vartheta}_{1dFL}\right)+\left(\upsilon_{FLeq}-\dddot{\vartheta}_{1dFL}\right)\end{aligned}\quad (15)$$

Let $\dot{s}_{FL}=0$, then the equivalent control υ_{FLeq} can be expressed by Eq. (16).

$$\upsilon_{FLeq}=\lambda_{FL}^2\dot{e}_{FL}+2\lambda_{FL}\ddot{e}_{FL}-\dddot{\vartheta}_{1dFL}\quad (16)$$

The function of switching the control is to drive the system state to approach the sliding mode switching surface $s_{FL}=0$; the output of the switching control is defined in Eq. (17).

$$\upsilon_{FLsw}=-\varepsilon_{FL}\,\mathrm{sgn}(s_{FL})\quad (17)$$

In Eq. (17), ε_{FL} is the switching constant and sgn(s_{FL}) is a sign function. Equation (14) can be expressed as:

$$\upsilon_{FL}=\lambda_{FL}^2\dot{e}_{FL}+2\lambda_{FL}\ddot{e}_{FL}-\dddot{\vartheta}_{1dFL}-\varepsilon_{FL}\,\mathrm{sign}(s_{FL})\quad (18)$$

Based on the Lyapunov stability condition, if the designed sliding mode control system is stable, the inequality (19) is correct.

$$\dot{V}(s_{FL})=\frac{1}{2}\frac{d}{dt}s_{FL}^2=s_{FL}\dot{s}_{FL}<-\eta_{FL}|s_{FL}|\quad (19)$$

In Eq. (19), η_{FL} is an arbitrarily small positive integer. The function of the equivalent control u_{FLeq} is to ensure that $\dot{s}_{FL}$ =0; therefore, Eq. (19) can be expressed as:

$$s_{FL}\left(-\varepsilon_{FL}\mathrm{sign}\left(s_{FL}\right)\right)<-\eta_{FL}\left|s_{FL}\right| \quad \Rightarrow \varepsilon_{FL}>\eta_{FL} \tag{20}$$

It is known from Eq. (20) that when $\varepsilon_{FL}>\eta_{FL}$, the sliding mode control system [29-30] is stable. In order to reduce the system chatter caused by the switching control in the auto load-levelling control system, the sign function in Eq. (17) can be replaced by the saturation function of Eq. (21).

$$\mathrm{sat}\left(s_{FL}/\psi_{FL}\right)=\begin{cases} s_{FL}/\psi_{FL}, & \left|s_{FL}\right|\le\psi_{FL} \\ \mathrm{sgn}(s_{FL}), & \left|s_{FL}\right|>\psi_{FL} \end{cases} \tag{21}$$

In Eq. (21), ψ_{FL} is the boundary layer thickness. According to Eq. (18), the output of the sliding mode controller in the linear state is obtained as shown in Eq. (22).

$$\upsilon_{FL}=\lambda_{FL}^2\dot{e}_{FL}+2\lambda_{FL}\ddot{e}_{FL}-\dddot{\vartheta}_{1dFL}-\varepsilon_{FL}\mathrm{sat}\left(s_{FL}/\psi_{FL}\right) \tag{22}$$

Combined with Eqs. (12) and (22), the actual sliding mode control amount of the front left air suspension inflation is as shown in Eq. (23).

$$u_{FL}=\frac{-\lambda_{FL}^2\dot{e}_{FL}-2\lambda_{FL}\ddot{e}_{FL}+\dddot{\vartheta}_{1dFL}-L_f{}^3h\left(\boldsymbol{x}_{FL}\right)-\varepsilon_{FL}\mathrm{sat}\left(s_{FL}/\psi_{FL}\right)}{L_gL_f{}^2h\left(\boldsymbol{x}_{FL}\right)} \tag{23}$$

Similarly, the actual sliding mode control amounts u_{FR}, u_{RL}, and u_{RR} of the front right, rear left, and rear right air suspension inflation processes are as shown in Eqs. (24)-(26), respectively.

$$u_{FR}=\frac{-\lambda_{FR}^2\dot{e}_{FR}-2\lambda_{FR}\ddot{e}_{FR}+\dddot{\vartheta}_{1dFR}-L_f{}^3h\left(\boldsymbol{x}_{FR}\right)-\varepsilon_{FR}\mathrm{sat}\left(s_{FR}/\psi_{FR}\right)}{L_gL_f{}^2h\left(\boldsymbol{x}_{FR}\right)} \tag{24}$$

$$u_{RL}=\frac{-\lambda_{RL}^2\dot{e}_{RL}-2\lambda_{RL}\ddot{e}_{RL}+\dddot{\vartheta}_{1dRL}-L_f{}^3h\left(\boldsymbol{x}_{RL}\right)-\varepsilon_{RL}\mathrm{sat}\left(s_{RL}/\psi_{RL}\right)}{L_gL_f{}^2h\left(\boldsymbol{x}_{RL}\right)} \tag{25}$$

$$u_{RR}=\frac{-\lambda_{RR}^2\dot{e}_{RR}-2\lambda_{RR}\ddot{e}_{RR}+\dddot{\vartheta}_{1dRR}-L_f{}^3h\left(\boldsymbol{x}_{RR}\right)-\varepsilon_{RR}\mathrm{sat}\left(s_{RR}/\psi_{RR}\right)}{L_gL_f{}^2h\left(\boldsymbol{x}_{RR}\right)} \tag{26}$$

In Eqs. (24) to (26), λ_{FR}, λ_{RL}, and λ_{RR} are the sliding mode coefficients corresponding to the respective suspension controls. ε_{FR}, ε_{RL}, and ε_{RR} are the switching constants. ψ_{FR}, ψ_{RL}, and ψ_{RR} are the boundary thicknesses.

In addition, in the case of an unbalanced load of the sprayer, the load on each chassis suspension will change. It is assumed that if the sprayer is operating in a certain extreme condition, the roll angle and the pitch angle are θ and φ, respectively. The distance from the barycentre to the front and rear axles are a and b, respectively. According to θ, φ, a, b and the overall mass m_s, the sprung mass of each sprayer chassis suspension in the limit working condition can be calculated by Eq. (27).

$$\begin{cases} m_{sFL}=m_s\left(\dfrac{b}{2L}-\dfrac{\theta}{2}+\dfrac{\varphi}{2}\right) \\ m_{sFR}=m_s\left(\dfrac{b}{2L}+\dfrac{\theta}{2}+\dfrac{\varphi}{2}\right) \\ m_{sRL}=m_s\left(\dfrac{a}{2L}-\dfrac{\theta}{2}-\dfrac{\varphi}{2}\right) \\ m_{sRR}=m_s\left(\dfrac{a}{2L}+\dfrac{\theta}{2}-\dfrac{\varphi}{2}\right) \end{cases} \tag{27}$$

In Eq. (27), m_{sFL}, m_{sFR}, m_{sRL}, and m_{sRR} are the sprung masses of each suspension.

In the actual auto load-levelling control process of the sprayer chassis air suspension, according to equations (23) - (26), the controlled quantity u_{ij} of proportional solenoid valve is obtained when the suspension is inflated and deflated, and then the opening degree of the proportional solenoid valve is controlled by pulse width modulation (PWM) method. The actual switching state duty ratio of the proportional solenoid valve can be obtained by Eq. (28).

$$u_{ijPWM}=\begin{cases}1, & \text{When} \quad u_{ij}\geq\left|u_{0maxij}\right|\\ u_{ij}\Big/\left|u_{0maxij}\right|, & \text{When} \quad 0<u_{ij}<\left|u_{0maxij}\right|\\ 0, & \text{When} \quad u_{ij}\leq 0\end{cases} \tag{28}$$

In Eq. (28), u_{ijPWM} is the duty ratio of the proportional solenoid valve actual switching state. u_{0maxij} is the product of the air mass flow and the unit control period when the solenoid valve is fully opened. The mass flow value required in the spring height control process can be converted into the duty cycle in the solenoid valve switch electrical signal, so as to control the solenoid valve more conveniently. The maximum control amount u_{0maxij} of each suspension can be obtained by equation (29).

$$u_{0maxij}=\begin{cases}c_d KA_{K1max}\,p_c N_c\Big/\sqrt{T_c} & \text{When the spring is inflated}\\ -c_d KA_{K1max}\,p_{1ij} N_k\Big/\sqrt{T_1} & \text{When the spring is deflated}\end{cases} \tag{29}$$

In Eq. (29), A_{k1max} is the solenoid valve port area when the proportional solenoid valve connected to the spring is fully opened.

RESULTS AND DISCUSSION

Matlab/Simulink was used to develop the simulation model of the auto load-levelling control system. The simulation used fixed-step type, and the solving algorithm used ode3 (Bogacki-Shampine). The sampling frequency was 1000Hz and the sampling time was 6s in the simulation. Simulation parameters are shown in Tab. 2.

Table 2

Initial simulation parameters of auto load-levelling control

Parameters / unit	Instructions	Values	Parameters / unit	Instructions	Values
m_s / kg	Body mass	12000	T_{ij} / K	Internal spring temperature	293
V / km·h^{-1}	Speed	12	f / Hz	Sampling frequency	1000
B_F / m	Wheel track	3.2	t / s	Sampling time	6
a / m	Front axle distance from centroid	1.8	λ_{ij}	Sliding mode coefficient of each suspension	40.328
b / m	Rear axle distance from centroid	2.2	ε_{ij}	Switching constant of each suspension	16
V_1'	Rate of change in volume of the spring	0.518	ψ_{ij}	Boundary thickness of each suspension	0.01
x_{0ij} / mm	Initial spring height	380	C_{sij} / N·s·m^{-1}	Suspension damping	2400
V_{10ij} / m^3	The initial working volume of the spring	0.01914	G / mm	Centroid height of sprayer	1620
m_{tij} / kg	Unsprung mass of each suspension system	300	k_{tij} / N·m^{-1}	Tire equivalent radial stiffness	560000
C_{tij} / N·s·m^{-1}	Tire equivalent radial damping	5700			

In order to verify the performance of the proposed sliding mode control method, the front left air suspension was increased by 0.08 m or reduced by 0.08 m from the design height of 0.38 m and the suspension height adjustments in the on-off control, PID control and sliding mode control were obtained, as shown in Fig. 6. The Ziegler-Nichols method was used to tune the PID controller parameters and selected the best PID control parameters. Through the tuning of PID control parameters, the proportional link coefficient k_P=25.4, the integral link coefficient k_I=15.8, and the differential link coefficient k_D=10.2. Fig. 6 (a) shows the lift of the front left air suspension. After 3 s, the target height of 0.46 m is reached under sliding mode control and the suspension heights in the on-off control and PID control are still being adjusted. After 3.5 s, the suspension height in the on-off control has stabilized at 0.47 m, exceeding the target height by 0.01 m. At this time, the height of the suspension under PID control accurately reaches the target height of 0.46 m. Fig. 6 (b) shows the lowering of the front left air suspension. After 3 s, the target height of 0.30 m is reached under sliding mode control. After 3.5 s, the suspension height in the on-off control has stabilized at 0.295 m, exceeding the target height by 0.005 m. At this time, the height of the suspension under PID control

accurately reaches the target height of 0.30 m. The simulation results show that both the sliding mode control and PID control have higher precision, and both effectively solve the problems of "overcharging" and "over discharging" in the suspension height control process. However, compared with PID control, sliding mode control has a faster response speed and better robustness for air suspension system with strong nonlinearity.

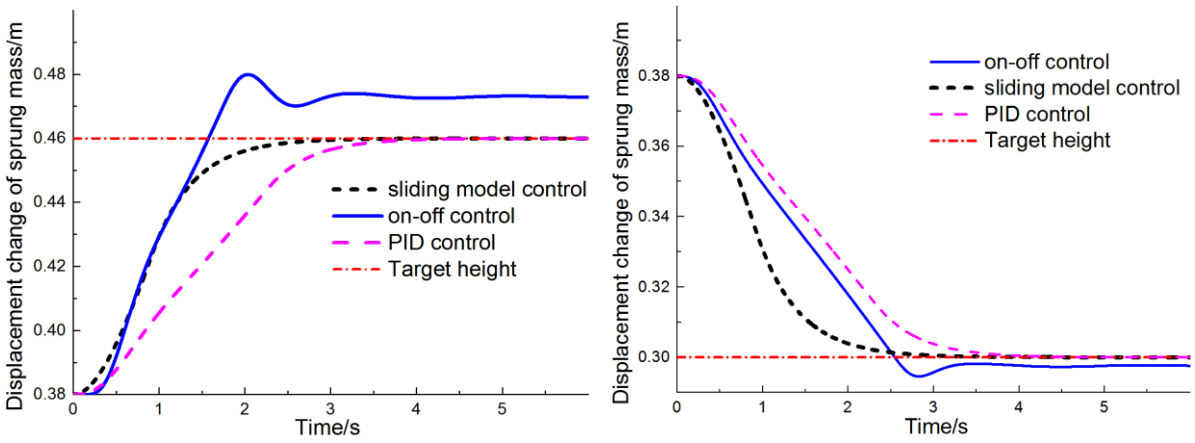

(a) The lift of the front left air suspension *(b) The lowering of the front left air suspension*

Fig. 6 - The suspension height adjustment effect in different control modes

In order to verify the performance of the auto load-levelling algorithm based on the sliding mode control, the sprayer is tested using different roll and pitch angles and rough road conditions; the roll angle, pitch angle, barycentre height, sprung mass of each suspension, and the height changes were analysed, as shown in Figs. 7-9. According to the sprayer auto load-levelling control strategy in Section 2.3.1 and the parameter data in Tab. 2, since the sprayer wheel track is 3.2m, the distance from the front axis to the centroid is 1.8m, the distance from the rear axis to the centroid is 2.2m, the centroid height is 1.62m, initial air spring height is 380mm, and the maximum height difference between the air springs should not exceed 160mm. By calculating the above parameters and obtaining that the maximum roll angle of the sprayer does not exceed 0.025rad, and the maximum pitch angle does not exceed 0.02rad.

Fig. 7 shows the changes in various parameters during auto load-levelling for a roll angle of 0.025 rad and a pitch angle of 0 rad. The auto load-levelling controller first deflated the two suspensions on the left side of the sprayer until the suspensions' heights were reduced from 2.08 m to 2.0 m. The heights of the two suspensions on the left and right sides were equal, as shown in Fig. 7(b). The body roll angle gradually decreased from 0.025 rad to 0 rad and the centroid height also decreased. The pitch angle fluctuated around 0 rad and the change was negligible, as shown in Fig. 7(a). When the suspension height on the left side changed, the load on each spring also changed; ultimately, the suspension's sprung mass on the left and right sides of the machine were equal and the load of each suspension reached an equilibrium state.

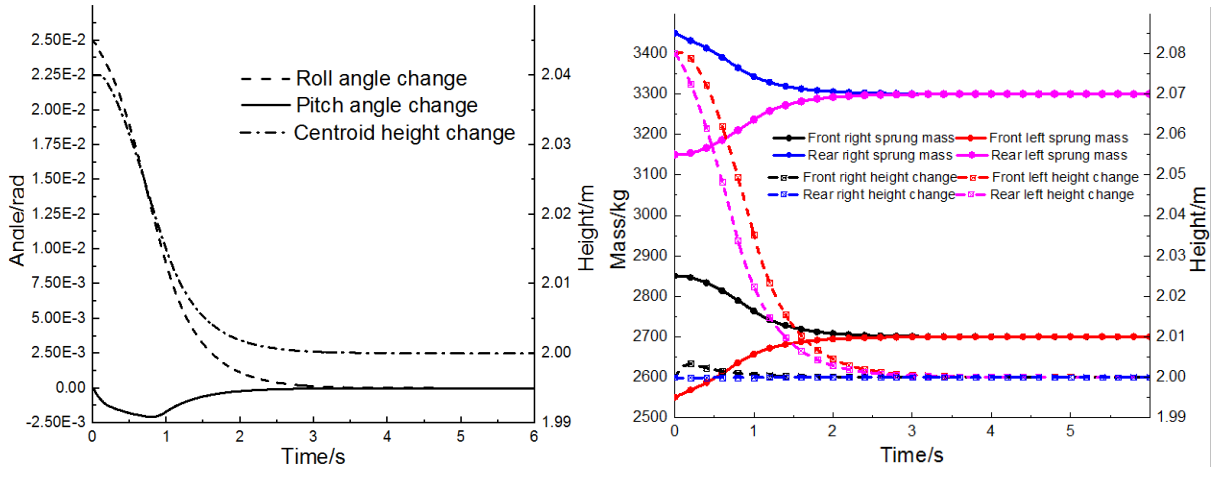

(a) Roll angle, pitch angle and centroid height changes *(b) Sprung mass and height changes*

Fig. 7 -Effect control of auto load-levelling during body rolling

Fig. 8 shows the changes in various parameters during auto load-levelling control for a roll angle of 0 rad and a pitch angle of 0.02 rad. Similar to the control process shown in Fig. 7, the auto load-levelling controller first deflated the two suspensions on the rear side of the sprayer until the suspensions' heights were reduced from 2.08 m to 2.0 m. The heights of the two suspensions on the front and rear sides were equal, as shown in Fig. 8(b).

The body pitch angle gradually decreased from 0.02 rad to 0 rad and the centroid height also decreased. The roll angle fluctuated around 0 rad and the change was negligible, as shown in Fig. 8(a). When the suspension height on the rear side changed, the load on each spring also changed; ultimately, the suspension's sprung mass on the front and rear sides of the machine were equal and the load of each suspension reached an equilibrium state.

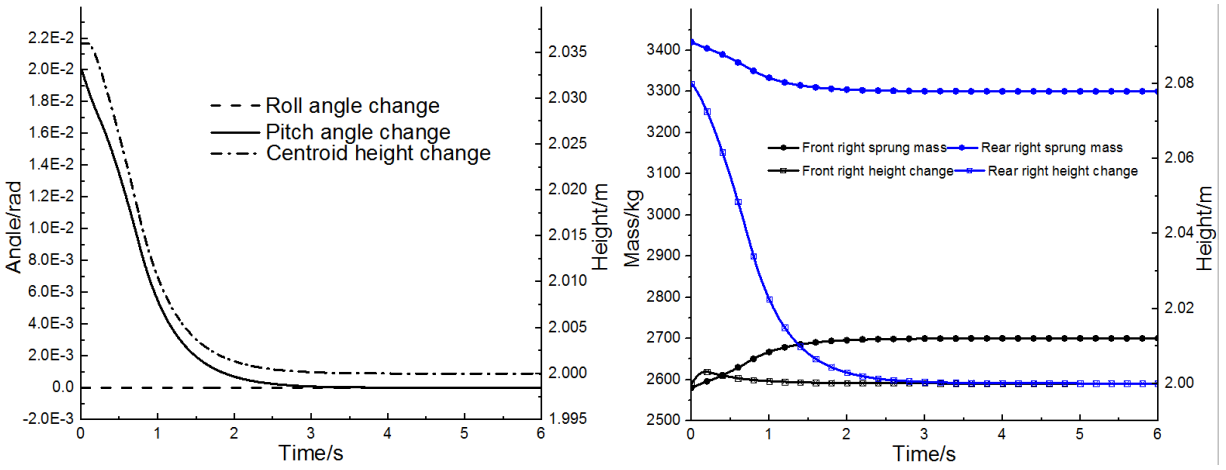

(a) Roll angle, pitch angle and centroid height changes *(b) Sprung mass and height changes*

Fig. 8 - Effect control of auto load-levelling during body pitching

Fig. 9 showed the changes in various parameters during auto load-levelling control for a roll angle of 0.025 rad and a pitch angle of 0.02 rad. The controller reduced the height of each suspension to 2.0 m. The auto load-levelling controller first inflated the front right suspension and deflated the other suspensions until all suspension heights reached the target height, as shown in Fig. 9(b).

The body roll angle and pitch angle gradually decreased from 0.025 rad and 0.02 to 0 rad, respectively. The centroid height also decreased, as shown in Fig. 9(a). Finally, the load on each suspension reached a balanced state.

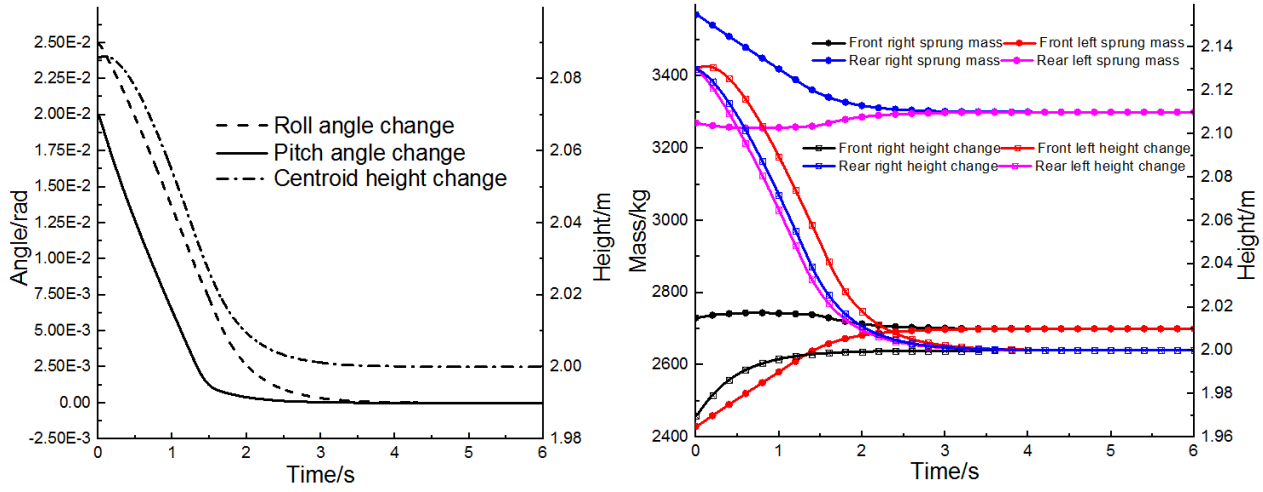

(a) Roll angle, pitch angle and centroid height changes *(b) Sprung mass and height changes*

Fig.9 - Effect control of auto load-levelling during sprayer running on the uneven road

CONCLUSIONS

During the sprayer operation, load imbalance will cause the wheels to slip or the machine to roll over, affecting the safe operation and handling stability of the sprayer. Auto load-levelling control is an important technology to improve sprayer performance. The following conclusions can be drawn:

(1) A model of the charge and discharge of the air suspension of a sprayer was established and a ¼-scale vertical dynamics model of the suspension was developed to lay a theoretical foundation for auto load-levelling control of a sprayer.

(2) The proposed auto load-levelling control algorithm with sliding mode effectively overcomes the problems of oscillation, "overcharging" and "over discharging" in the vehicle height control process, and has good accuracy, good control response and robustness to changes in the model parameters.

(3) The control strategy and algorithm meet the needs of auto load-levelling control and provide reference information for auto load-levelling control of self-propelled sprayers.

However, the above research mainly verified the proposed auto load-levelling control effect of the large self-propelled sprayer from a simulation perspective. Although the implementation method of applying pulse width modulation (PWM) to the proportional solenoid valve opening control in actual control was also proposed, its actual control effect needs to be further verified. In addition, since the high control activity of the sliding mode control method is the main factor restricting its practical application, it is necessary to further study the sliding mode control problem of the discrete-time system, the optimization problem of the sliding mode control parameters, or combined the sliding mode control with other control methods, such as fuzzy control for joint control to overcome the shortcomings of the current sliding mode control method, so as to better realize the auto load-levelling control actual vehicle application of the large self-propelled sprayer chassis air suspension.

ACKNOWLEDGMENT

The authors thank the editing team of EditorBar for improving the English language fluency of our paper. The work in this paper was supported by the Key Research and Development Program of Shaanxi Province (No. 2019ZDLNY02-01), the National Key Research and Development Program (No.2018YFD0701100-2018YFD0701102) and the China Postdoctoral Science Foundation (No.2018M643744).

REFERENCES

[1] Assadsangabi B., Eghtesad M., Daneshmand F., Vahdati N., (2009), Hybrid sliding mode control of semi-active suspension systems, *Smart Materials and Structures*, vol.18, pp.406-414.

[2] Baumhardt U. B., Airton D. S. A., Tenorio H. G. T., Ferreira C. C., Bedin P. R., (2017), Methodology for conception of cabins of agricultural machines: informational phase applied to a self-propelled sprayer, *Journal of the Brazilian Society of Mechanical Sciences and Engineering*, vol.39, pp.1683-1694.

[3] Carlson B. C., Young D. E., Baxter G. E., Anderson J. C., (2011), *Suspended axle for sprayer*, US, Patent 7938415.

[4] Carneiro J. F., De A. F. G., (2006), Reduced-order thermodynamic models for servo-pneumatic actuator chambers, *Proceedings of the Institution of Mechanical Engineers*, Part I: Journal of Systems and Control Engineering vol.220, pp.301-314.

[5] Chen Y., Chen L., Xu X., Huang C., (2015), Vehicle height control of electronic-controlled air suspension under random disturbance（随机干扰下电控空气悬架整车车身高度控制研究）, *Transactions of the Chinese Society for Agricultural Machinery*, vol.46, pp.309-315.

[6] Chen Y., Chen S., Du Y., Zhu Z., Mao E., (2016), Damping characteristics of chassis suspension system of high clearance agricultural machinery based on friction damper（基于摩擦阻尼的高地隙农机底盘悬架减振特性）, *Transactions of the CSAE*, vol.32, pp.51-57.

[7] Chen Y., Mao E., Li W., Zhang S., Song Z., Yang S., Chen J., (2020), Design and experiment of a high-clearance self-propelled sprayer chassis, *International Journal of Agricultural and Biological Engineering*, vol.13, pp.71-80.

[8] Chen Y., Zhang S., Mao E., Du Y., Chen J., Yang S., (2020), Height stability control of a large sprayer body based on air suspension using the sliding mode approach, *Information Processing in Agriculture* vol.7, pp.20-29.

[9] Cui L., Mao H., Xue X., Ding S., Qiao B., (2018), Optimized design and test for a pendulum suspension of the crop spray boom in dynamic conditions based on a six DOF motion simulator, *International Journal of Agricultural and Biological Engineering*, vol.11, pp.76-85.
[10] Cui L., Xue X., Ding S., Le F., (2019), Development of a DSP-based electronic control system for the active spray boom suspension, *Computers and Electronics in Agriculture*, vol.166, pp.1-9.
[11] Cui L., Xue X., Le F., Mao H., Ding S., (2019), Design and experiment of electro hydraulic active suspension for controlling the rolling motion of spray boom, *International Journal of Agricultural and Biological Engineering*, vol.12, pp.72-81.
[12] Gil E., Gallart M., Balsari P., Marucco P., Almajano M., Llop J., (2015), Influence of wind velocity and wind direction on measurements of spray drift potential of boom sprayers using drift test bench, *Agricultural and forest meteorology*, vol.202, pp.94-101.
[13] Herbst A., Osteroth H., Stendel H., (2018), A novel method for testing automatic systems for controlling the spray boom height, *Biosystems Engineering*, vol.174, pp.115-125.
[14] Holbrook G. (2010), *Method and system for adjusting a vehicle aligned with an artificial horizon*, EP, 7744099.
[15] Ilica A., Boz A., (2018), Design of a nozzle-height control system using a permanent magnet tubular linear synchronous motor, *Journal of Agricultural Sciences*, vol.24, pp.374-385.
[16] Jang I., Kim H., Lee H., Han S., (2007), Height control and failsafe algorithm for closed loop air suspension control system, *2007 International Conference on Control, Automation and Systems*, Seoul, pp.373-378.
[17] Jiang H., Yang Y., Wang Y., Xu X., Li M., (2017), Experimental study on height control and energy consumption characteristics of closed-loop air circuit interconnected air suspension system（气路闭环互联空气悬架车高控制与能耗特性试验）, *Journal of Central South University (Science and Technology)*, vol.48, pp.270-276.
[18] Jiang H., Yang Y., Xu P., Xu X., Li M., (2015), Vehicle height adjustment of closed-loop air circuit laterally interconnected air suspension system（气路闭环横向互联空气悬架车身高度调节）, *Journal of Beijing University of Aeronautics and Astronautics*, vol.41, pp.2010-2016.
[19] Jin M., Lee J., Ahn K., (2014), Continuous nonsingular terminal sliding-mode control of shape memory alloy actuators using time delay estimation, IEEE/ASME *Transactions on Mechatronics*, vol.20, pp.899-909.
[20] Kim H., Lee H., (2011), Fault-tolerant control algorithm for a four-corner closed-loop air suspension system, *IEEE transactions on industrial electrics*, vol.58, pp.4866-4879.
[21] Kim H., Lee H., (2011), Height and levelling control of automotive air suspension system using sliding mode approach, *IEEE transactions on industrial electrics*, vol.60, pp.2027-2041.
[22] Li W., Chen Y., Zhang S., Mao E., Du Y., Wen H., (2018), Damping characteristic analysis and experiment of air suspension with auxiliary chamber, *IFAC-PapersOnLine*, vol.51, pp.166-172.
[23] Li X., Wei X., Jia L., Chen X., Liu L., Zhang Y., (2017), Recognition of Crops, Diseases and Pesticides Named Entities in Chinese Based on Conditional Random Fields（基于条件随机场的农作物病虫害及农药命名实体识别）, *Transactions of the Chinese Society for Agricultural Machinery*, vol.48, pp.178-185.
[24] Melzi S., Negrini S., Sabbioni E., (2014), Numerical analysis of the effect of tire characteristics, soil response and suspensions tuning on the comfort of an agricultural vehicle, *Journal of Terramechanics*, vol.55, pp.17-27.
[25] Porumamilla H., Kelkar A., (2005), Robust control and μ analysis of active pneumatic suspension, *2005 American Control Conference*, pp.2200-2205.
[26] Schaffer J., (2002), *Steering system for variable height agricultural sprayer*. US, Patent 6371237.
[27] Schaffer J., (2002), *Wheel support system for agricultural sprayer*, US, Patent 6491306.
[28] Tahmasebi M., Gohari M., Mailah M., Abd R., (2018), Vibration suppression of sprayer boom structure using active torque control and iterative learning, part ii: experimental implementation, *Journal of Vibration and Control*, vol.24, pp.4740–4750.
[29] Tahmasebi M., Mailah M., Gohari M., Abd R., (2018), Vibration suppression of sprayer boom structure using active torque control and iterative learning, part i: modelling and control via simulation, *Journal of Vibration and Control*, vol.24, pp.4689–4699.

[30] Tahmasebi M., Rahman R., Mailah M., Gohari M., (2013), Roll movement control of a spray boom structure using active force control with artificial neural network strategy, *Journal of Low Frequency Noise Vibration and Active Control*, vol.32, pp.189–201.

[31] Wang S., Chen L., Sun X., (2013), A multi-mode switching control mode for semi-active air suspension（半主动空气悬架多模式切换控制模型的分析），*Journal of Jiangsu University (Natural Science Edition)*, vol.34, pp.637-642.

[32] Wang S., Dou H., Sun X., Yin C., (2015), Vehicle height adjustment and attitude control of electronically controlled air suspension（电控空气悬架车高调节与整车姿态控制研究），*Transactions of the Chinese Society for Agricultural Machinery*, vol.46, pp.335-342+356.

[33] Wubben T., Maiwald M., Carlson B., Anderson J., (2007), *High clearance vehicle suspension with twin spindles for transferring steering torque*, US, Patent 7168717.

[34] Yang Q., (2008), *Research on matching and inflation/deflating of suspension system in ECAS-Bus*（ECAS客车悬架系统的匹配与充放气研究）, Zhenjiang: Jiangsu University.

[35] Yuki S., Yasuda H., Matsubayashi T., Ishizhka H., (2013), Development of tractor automatic controlled boom sprayer using CAN-BUS, *IFAC Proceedings Volumes*, vol.46, pp.264-269.

[36] Zatrieb J., Kasler R., (2012), New generation of hydro-pneumatic suspension systems with adaptive damping, *SAE Technical Paper*, 2012-36-0016.

[37] Zhao Y., Wang Z., Chen S., (2014), Investigation of height control for air suspension system based on sliding mode method（基于滑模控制的空气悬架车高控制系统研究），*Transactions of Beijing Institute of Technology*, vol.34, pp.1125-1129.

[38] Zirkohi M., Lin T., (2015), Interval type-2 fuzzy-neural network indirect adaptive sliding mode control for an active suspension system, *Nonlinear Dynamics*, vol.79, pp.513-526.